

Quantitative Heat Dissipation Characteristics in Current-Carrying GaN Nanowires Probed by Combining Scanning Thermal Microscopy and Spatially Resolved Raman Spectroscopy

Afsoon Soudi, Robert D. Dawson, and Yi Gu*

Department of Physics and Astronomy, Washington State University, Pullman, Washington 99164, United States

With the continued decrease of the feature size, accompanied by the increase in device and power density in integrated circuits, managing heat generation and dissipation in the nanoscale becomes increasingly important to reliable circuit operations.^{1–3} The development of effective thermal management schemes, to a large extent, depends on an understanding of heat dissipation and transfer characteristics in individual devices. Recently, semiconductor nanowires have been extensively explored as active device elements in nanoscale electronics. In particular, group III nitride nanowires have shown enormous potential in optoelectronic applications, such as light-emitting diodes^{4,5} and lasers.^{6,7} These devices often operate at high power levels. Elevated temperatures, due to Joule heating, can be detrimental to device performance.⁸ This issue might be more significant in nanowire-based devices due to reduced thermal conductivities.^{9,10} Therefore, a quantitative knowledge of heat dissipation and transfer characteristics in these nanowires, especially when they are configured as active current-carrying elements, is central to developing effective cooling schemes and realizing envisioned applications. From a more fundamental perspective, studies of these characteristics can provide insight into how one-dimensional phonon confinement modifies thermal transport properties of these nanowires.

The heat dissipation and transfer properties can be obtained by analyzing the spatial variations of temperature in the active device region. A recent study¹¹ used a

ABSTRACT Using an approach combining scanning thermal microscopy (SThM) and spatially resolved Raman spectroscopy, we have investigated quantitatively the heat dissipation characteristics in substrate-supported and suspended (with asymmetric type of contacts) current-carrying GaN nanowires with diameters of ~ 40 – 60 nm, where the phonon confinement is expected to play an important role in thermal transport. In particular, this approach allows direct measurements of nanowire–substrate/electrode interface thermal resistances and the nanowire thermal conductivity. On the basis of these results, the nanowire–substrate thermal transfer was suggested to be the main heat dissipation route, counting for ~ 80 – 93 % of the total dissipated heat, whereas the nanowire–electrode interface plays a minor role. The relative significance of nanowire-substrate/electrode interfaces in dissipating heat was further demonstrated in suspended nanowire devices. The measured nanowire thermal conductivity (~ 40 – 60 W/mK) is lower than that in bulk GaN, possibly due to the phonon confinement and boundary scattering effects. Besides providing quantitative insight into heat dissipation characteristics, our results also reveal aspects, particularly the topography-related thermal signals and the relative significance of various tip–sample thermal transfer processes, that are important to advancing the applications of SThM technique in nanoscale thermal characterizations.

KEYWORDS: nanowires · scanning thermal microscopy · Joule heating · heat dissipation · Raman scattering spectroscopy

model based on photoluminescence as a function of temperature to predict the temperature profile along large-diameter (>200 nm) GaN nanowires. This approach provided useful information on nanowire thermal conductivity and thermal resistance at the nanowire–substrate interface; however, direct measurements of temperature variations at nanoscale are desirable for enabling unambiguous and quantitative insight into heat dissipation and transfer characteristics. In addition, the thermal resistance at the nanowire–electrode interface might also be significant in contributing to the overall heat dissipation; this is also important for standard nanowire thermal conductivity measurements using the suspension configuration, where the

*Address correspondence to
yigu@wsu.edu.

Received for review October 4, 2010
and accepted December 03, 2010.

Published online December 14, 2010.
10.1021/nn102818s

© 2011 American Chemical Society

nanowire–electrode (contact) thermal resistance, often ignored, can lead to significant errors.¹²

For the direct measurement of temperature spatial variations, several techniques have been demonstrated,^{13,14} including scanning thermal microscopy (SThM),¹⁵ micro-Raman spectroscopy,^{16–18} infrared imaging,^{19,20} and laser reflectance thermometry.^{21,22} Compared to the far-field optical techniques, SThM, usually implemented on atomic force microscopes (AFM) working in the contact mode, provides beyond diffraction limit spatial resolutions,^{23,24} such capabilities are highly desirable for resolving temperature variations within individual nanoscale objects. Particularly, SThM with the spatial resolution of ~ 50 –100 nm has been applied to probing energy dissipation in Joule-heated carbon nanotubes.²⁵ With a known nanotube thermal conductivity, those studies allowed the evaluation of the thermal resistances at both nanotube–substrate and nanotube–electrode interfaces.²⁶ However, in many nanomaterial systems, the thermal conductivity is usually not well-known. Therefore, it is rather difficult to obtain quantitative information based on SThM studies alone.

Here, we have investigated quantitatively the heat dissipation and transfer characteristics in individual current-carrying GaN nanowires using SThM combined with spatially resolved Raman spectroscopy. We focus on nanowires with small diameters (40–60 nm), where the confinement of acoustic phonons that carry most of heat is pronounced^{9,10} and expected to play a critical role in thermal transport. By analyzing the directly measured temperature profiles along both substrate-supported and suspended nanowire devices, and combining SThM results with spatially resolved Raman spectra, we have quantified the relative contributions from nanowire–substrate and nanowire–electrode thermal transfer to the total heat dissipation, thermal resistances at the nanowire–substrate and nanowire–electrode interfaces, and nanowire thermal conductivity. Our results also reveal aspects, particularly the topography-related thermal signals and the relative significance of various tip–sample thermal transfer processes, that are important to advancing the applications of SThM technique in nanoscale thermal characterizations.²⁶ In addition, the approach of combining SThM and spatially resolved Raman spectroscopy, as demonstrated here, can play an important role in bringing a quantitative understanding to heat dissipation and thermal transport in nanoscale devices in general.

RESULTS AND DISCUSSION

The synthesis of GaN nanowires was described in detail elsewhere²⁷ (see also the Methods section). Single GaN nanowire two-terminal devices were fabricated on silicon substrates coated with a silicon nitride (Si_3N_4) layer (~ 400 nm thick). The Si_3N_4 layer was chosen be-

cause it is increasingly being used as the gate material in GaN-based field-effect transistors (FETs).^{28,29} As “hot spots” often develop under the gate in FET structures,^{3,15} a quantitative knowledge of the thermal transport across the GaN and Si_3N_4 interface, particularly the thermal boundary resistance, is of practical significance. The fabrication of suspended nanowire devices follows the procedure described in ref 30 (see also the Methods section). For the SThM studies, we note that while the diameter of SThM probes used here typically ranges from 150 to 200 nm, larger than the resolution (50–100 nm) that has been achieved with thermocouple probes,²⁵ the measured temperature profile along nanowires (with the length of 4–8 μm) is expected to approximately reflect the temperature variations in nanowires. The intermittent contact mode was used, which was necessary to minimize the mechanical interaction between nanowires and the probe; this was especially important for studying suspended nanowire devices.

Thermal images (without filtering or averaging) of a 40 nm diameter GaN nanowire device, under ac and dc biases, in ambient air, are shown in panels b and c of Figure 1, respectively. In particular, for the ac bias condition, a sinusoidal voltage with a dc offset $v = V_{\text{DC}} + V_{\text{DC}} \sin 2\pi ft$ ($f = 500$ Hz) was applied across the device, and the thermal signal (ΔV_{th}) was detected using the lock-in technique. To exclude the possibility of electrical coupling between the SThM probe and nanowires, we applied the same voltage on the two electrodes, in which case no thermal signal was observed. Furthermore, ΔV_{th} follows a parabolic relation to V_{rms} (the root-mean-square voltage of the ac bias), as shown in the inset to Figure 1b, verifying that ΔV_{th} is a measure of dissipated power and thus the temperature of the nanowire. This parabolic relation also indicates diffusive phonon transport, as expected, since the effective phonon mean free path in nanowires is usually comparable to the nanowire diameter.^{31,32} While the dc image shows essentially the same temperature variations as the ac image, the noise level is much higher. We therefore conducted the rest of experiments using the ac bias mode. The close similarity between the dc and ac temperature profiles allowed us to use a steady-state analysis (see also below).

Before analyzing the temperature profiles along nanowires, we first would like to discuss several relevant aspects that are important to applying the SThM technique to nanowire thermal characterizations. Particularly, it is well-known that topographical features often lead to artifacts in thermal images.¹⁵ Such artifacts appear to be negligible in the case of carbon nanotubes,^{25,33} for semiconductor nanowires with diameters on the order of tens of nanometers, however, topography-related artifacts can be rather significant. Here, we have observed a “double-line”-like feature in all thermal images, with one example shown in Figure

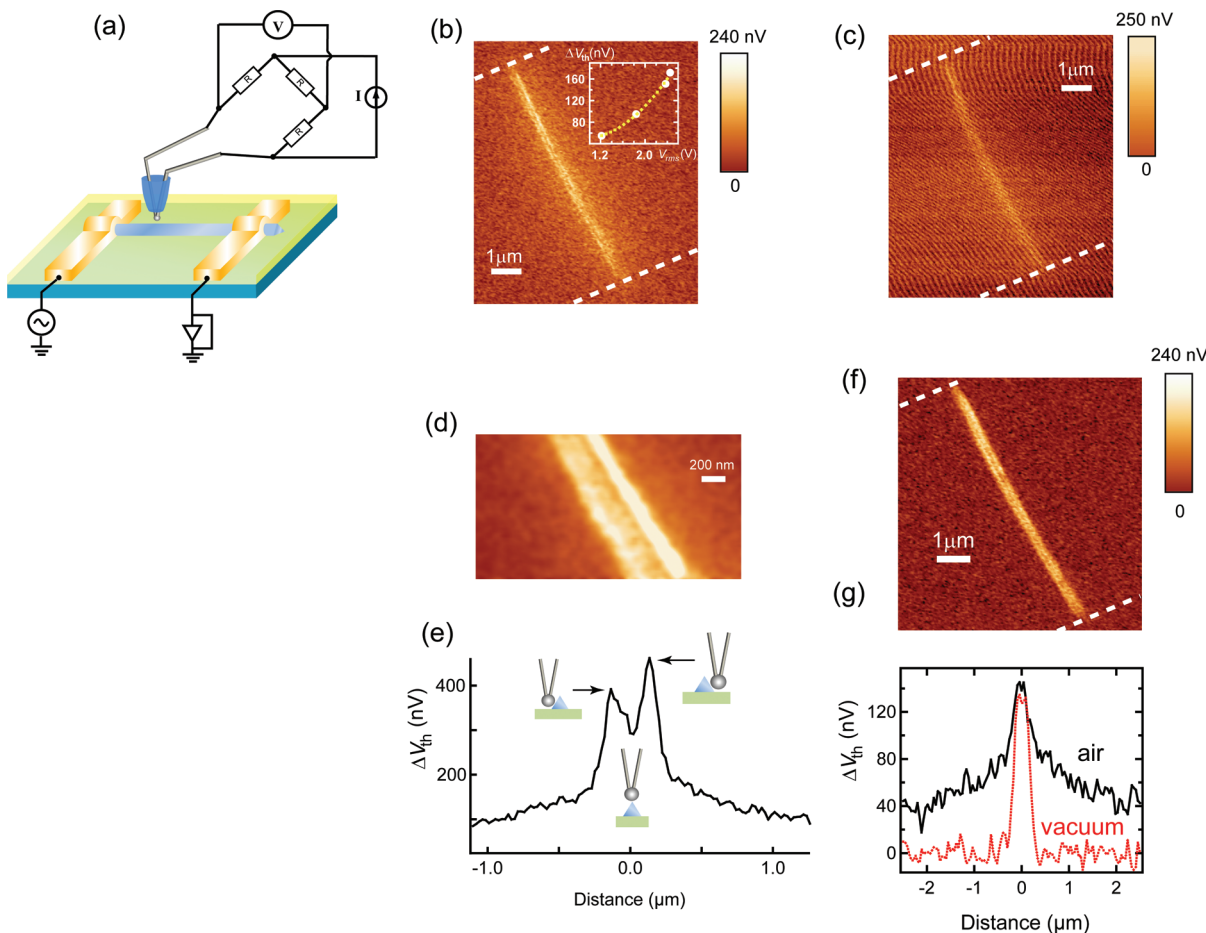


Figure 1. (a) Schematics of the SThM experiments; (b) ac and (c) dc SThM images with the inset to (b) showing the measured ΔV_{th} (solid circles) as a function of V_{rms} and the parabolic fitting (dashed line); (d) SThM images showing the “double-line”-like structure and (e) the corresponding profile across the nanowire; (f) SThM image obtained in vacuum ($\sim 10^{-6}$ Torr); (g) profiles of ambient and vacuum SThM images taken perpendicular to the nanowire.

1d,e. Specifically, a darker region (with a smaller ΔV_{th}) is sandwiched between two brighter lines (with a larger ΔV_{th}) in the perpendicular direction to the nanowire. We suggest that this is due to the triangular cross section of GaN nanowires: when the tip is on the top of the apex, the thermal coupling between the tip and the nanowire is rather poor compared to that when the tip is on one of nanowire facets, leading to a lower ΔV_{th} . Measurements on nanowires without such a triangular cross section will elucidate the nature of this feature and are currently underway. Nonetheless, the temperature profiles *along* the nanowire measured from these regions show the same spatial variations (not shown here), we thus used the averaged ΔV_{th} across the nanowire to represent the local temperature.

Another important aspect relevant to SThM thermal characterizations is the relative significance of various tip–sample heat transfer mechanisms, which plays an important role in determining the spatial resolution and is critical to quantifying SThM results. In particular, under ambient condition, heat conduction through air, a liquid film bridging the tip and the sample surface, solid–solid contact, and the radiative heat transfer are

the possible mechanisms. It has been shown that,^{23,34} for submicrometer-size features, liquid conduction is the dominant mechanism. A recent study²⁶ demonstrated that, in addition to the liquid conduction, the solid–solid conduction also plays an important role. In those studies, air and radiative conductances were found to play a less important but nontrivial role. Here, Figure 1f shows a SThM image obtained in high vacuum ($\sim 10^{-6}$ Torr). This can be directly compared to Figure 1b, as both images were obtained under otherwise the same conditions using the same thermal probe. It is obvious that, from Figure 1g, a slow-varying background signal away from the nanowire, which is the heat source, is present in the ambient SThM image, whereas such a feature is absent in the vacuum. As the heat conduction through the air is relatively insensitive to the distance between the tip and the heat source,²⁶ we suggest that this background signal is dominated by the air conduction between the SThM probe and the nanowire.³⁵ This is consistent with the presence of this background signal also in ambient SThM images of suspended nanowire devices (see also below). For the thermal signal obtained directly on the nanowire, how-

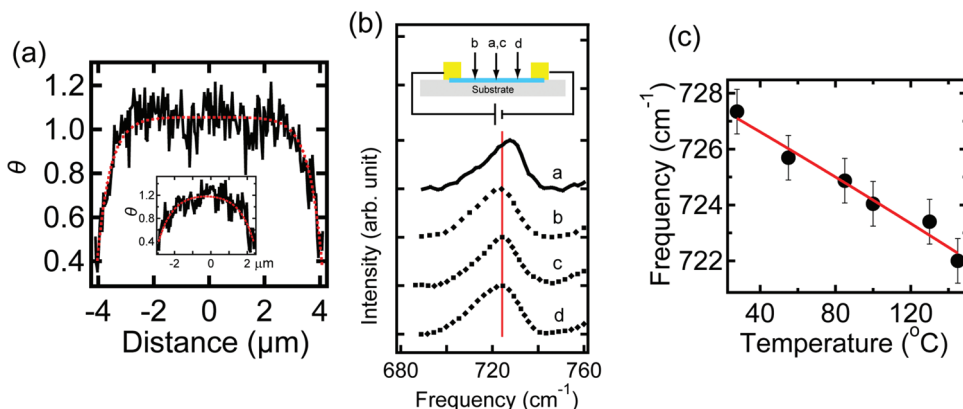


Figure 2. (a) Temperature (θ) profiles (black solid lines) along nanowires and the fitting results (red dotted lines) using eq 2; (b) spatially resolved Raman spectra of the A_1 LO phonon mode with spectrum a taken under the zero-bias (power) condition and spectra b–d taken along the biased nanowire with positions indicated in the inset, and the spectra are shifted vertically for clarity; (c) frequency of the A_1 LO phonon mode measured (solid circles) on a single nanowire as a function of the ambient temperature with the red solid line representing the fitting result.

ever, there is little difference ($\sim 5\%$) in the signal strength between the ambient and the vacuum images. This is in sharp contrast to previous studies,³⁴ where the thermal signal was found to decrease more than an order of magnitude in vacuum ($\sim 10^{-5}$ Torr), due to diminished liquid conduction. Since solid–solid and radiative conductions are the dominant heat transfer mechanisms in vacuum,^{36,37} our results suggest that, under ambient condition, these two processes also dominate the observed thermal signals measured on the nanowire.³⁸ A potentially important implication of these results is that, for experiments conducted in ambient, while the air conduction deteriorates the lateral spatial resolution (perpendicular to the nanowire), the spatial resolution of temperature variations along the nanowire should be mostly limited by the size of the thermal probe, as both solid–solid and radiative (in this case, most likely the near-field radiation) conductions are expected to be short-range interactions.^{39,40} Therefore, although vacuum SThM has been suggested to yield higher spatial resolutions,⁴¹ the ambient SThM, at least in our case, is expected to achieve the same spatial resolution along the nanowire.

Next we discuss the quantitative aspects of thermal images. In substrate-supported devices, the temperature profile is relatively constant along the most part of the nanowire. For the quantitative analysis, we follow the model described in ref 25. Particularly, with one-dimensional diffusive heating at steady state, we have

$$kA \frac{\partial^2 T(x)}{\partial x^2} + \frac{Q}{L} - G \times W \times [T(x) - T_0] = 0 \quad (1)$$

where k , A , $T(x)$, T_0 , Q , L , G , and W are the nanowire thermal conductivity, cross section area, local temperature on the nanowire, ambient temperature, total heating rate, device channel length, nanowire–substrate thermal conductance per unit area, and the width of the nanowire, respectively.⁴² The solution, with $x = 0$ at the middle of the channel, is given by²⁵

$$\begin{aligned} \theta(x) = \frac{T(x) - T_0}{T_{\text{avg}} - T_0} = q \times \left[1 - \frac{\cosh(mx)}{\cosh\left(\frac{mL}{2}\right)} \right] + \\ \frac{(T_{e,1} - T_0) + (T_{e,2} - T_0)}{2(T_{\text{avg}} - T_0)} \times \frac{\cosh(mx)}{\cosh\left(\frac{mL}{2}\right)} + \\ \frac{T_{e,2} - T_{e,1}}{2(T_{\text{avg}} - T_0)} \times \frac{\sinh(mx)}{\sinh\left(\frac{mL}{2}\right)} \end{aligned}$$

with

$$q = \frac{Q}{LGW(T_{\text{avg}} - T_0)}, \text{ and } m = \sqrt{\frac{GW}{kA}} \quad (2)$$

where T_{avg} is the average temperature along the nanowire, with $T_{e,1}$ and $T_{e,2}$ being the temperatures at the interface between nanowire and the two electrodes. The fitting of the measured temperature file using this relation is plotted in Figure 2a. The inset shows the fitting to a temperature profile obtained on a short-channel (~ 5 μ m) device. The curvature of the temperature profile is controlled by m , while q mostly determines the magnitude. From the values of q and m obtained from the fitting, G and k , the parameters of interest here, can be directly obtained if the absolute value of $T_{\text{avg}} - T_0$ is known. To obtain this value from SThM images requires a quantitative knowledge of the thermal resistance at the tip–nanowire junction, which, as a convoluted function of sample surface and ambient conditions (e.g., humidity) as well as sample topography, is very difficult to quantify.²⁵ In ref 25, the values of previously measured carbon nanotube thermal conductivity were used to estimate G . Here, however, k of GaN nanowires with a diameter of ~ 40 – 60 nm is unknown and is the parameter to be determined.

To address this issue, we used spatially resolved Raman spectroscopy for the measurement of $T_{\text{avg}} - T_0$ via lattice phonon modes. It is well-known that the frequencies of lattice phonons decrease with the increas-

ing temperature.^{43,44} Figure 2b shows Raman spectra of the A_1 longitudinal optical (LO) phonon mode taken from various locations on the nanowire device channel. Particularly, compared to the spectrum (a) taken without any bias (*i.e.*, without any Joule heating), the frequency of the A_1 LO phonon mode (ω_{LO}) shifts to lower values when the nanowire is biased. This frequency shift is uniform along most of the nanowire channel, consistent with SThM results.⁴⁵ We have also measured Raman spectra in nanowire channel regions right next to the electrodes (not shown here), and we observed a larger decrease in ω_{LO} , indicating higher temperatures in these regions. This is in conflict with SThM results showing lower temperatures close to the electrodes. We believe that this is due to the optical absorption of laser energy by the metal electrodes, which leads to a temperature increase in the electrodes as well as the adjacent nanowire regions. This suggests that, while Raman spectroscopy can enable a direct measurement of temperature, it has limited capabilities in resolving temperature variations closed to metal contacts, which might contain important information on heat dissipation characteristics. To relate the shift in ω_{LO} to the temperature change, we carried out variable-temperature Raman on a single GaN nanowire. Figure 2c shows ω_{LO} measured (solid circles) at various temperatures. A model, which takes into account the thermal expansion, three-phonon, and four-phonon anharmonic coupling processes (see Supporting Information), was used to fit (solid line in Figure 2c) ω_{LO} as the function of temperature. The obtained fitting parameters allow us to calculate the temperature from any shift in ω_{LO} . With nanowire devices powered similarly (in the range of 100–400 μ W) for SThM and Raman studies, we obtained $T_{avg} - T_0$ (ranging from \sim 35 to 120 K).⁴⁶

With this, we estimated k to be \sim 50–60 W/mK and G to be $(\sim$ 0.3–2.0) \times 10⁷ W/m²K across various nanowire devices.⁴⁷ For comparison, the k of bulk GaN⁴⁸ depends on the doping level (n_e): with n_e increasing from \sim 10¹⁷ to 10¹⁹ cm⁻³, k decreases from \sim 200 to 75 W/mK. In addition, a previous study,⁹ which used the micro-heating technique with a suspended configuration, measured k of GaN nanowires (with diameters $>$ 97 nm) to be \sim 13–19 W/mK. The low k obtained was attributed to a large mass-difference scattering rate primarily due to the presence of Si impurity atoms.⁹ Here, with an estimated $n_e \sim$ 10¹⁸ cm⁻³, the values of measured k are below the corresponding bulk value (\sim 110 W/mK), possibly due to the phonon confinement and boundary (surface) scattering effects. While there is a likely presence of extended defects (*e.g.*, stacking faults), as suggested for GaN nanowires grown by the thermal chemical vapor deposition process,⁴⁹ such defects were shown to play a minor role in limiting the room temperature k .⁹ On the other hand, these values of k are higher than those obtained in larger-diameter GaN nanowires.⁹ This could be due to a lower n_e as a re-

sult of the absence of Si impurity atoms (assuming that the origin of these impurities is the Si substrates used for nanowire growth⁵⁰), which are donors in GaN, as well as a weaker mass-difference scattering. With regard to G , while, to the best of our knowledge, there is no literature results for the GaN/Si₃N₄ interface, the values obtained here [$(\sim$ 0.3–2.0) \times 10⁷ W/m²K] fall into the range of those determined for GaN/Si [$(\sim$ 1.4–3.0) \times 10⁷ W/m²K],^{51,52} GaN/SiC [$(\sim$ 0.8–3.0) \times 10⁷ W/m²K],^{51,52} and GaN/sapphire [$(\sim$ 0.2–1.0) \times 10⁷ W/m²K] interfaces.^{52–54}

On the basis of the fitting results and the obtained k and G , we next discuss the heat dissipation in GaN nanowires. The rate of heat dissipated from the nanowire into two metal electrodes, Q_e , can be written as²⁵

$$\frac{Q_e}{Q} = \frac{2 \left[1 - \frac{(T_{e,1} - T_0) + (T_{e,2} - T_0)}{2(T_{avg} - T_0)q} \right] \times \tanh\left(\frac{mL}{2}\right)}{mL} \quad (3)$$

This ratio, in general, decreases (from \sim 20 to \sim 7%) with increasing nanowire channel length (from 4 to 8 μ m). In any case, this rather small ratio suggests that the majority of the heat is transferred out of the nanowire into the substrate, although for shorter-channel devices, the heat transfer into the electrodes might begin to play a more important role. This heat dissipation characteristic can be understood from the thermal resistances at the nanowire–substrate ($R_{i,s}$) and nanowire–electrode ($R_{i,e}$) interfaces. In particular, $R_{i,e}$ is given²⁵ by $[(T_{e,1} - T_0) + (T_{e,2} - T_0)]/Q_e$, and, on average, was estimated to be \sim 4 \times 10⁶ K/W. $R_{i,s}$ can be obtained directly by $1/GWL$ and is in the range of (0.5–1.1) \times 10⁶ K/W. As $R_{i,e}$ is larger than $R_{i,s}$, more heat is dissipated through the substrate. We note that both $R_{i,e}$ and $R_{i,s}$ are much smaller than the nanowire thermal resistance, R_{hw} , given by L/ka , which is on the order of 10⁸ K/W.

To further illustrate the dominant role of the nanowire–substrate heat dissipation, we conducted studies on suspended nanowire devices. This suspended geometry, from the heat dissipation perspective, is similar to the fin-type field-effect transistors.^{3,55} Due to the gravity, suspended GaN nanowires are curved, and the midsection of the nanowire is in contact with the substrate, as illustrated in Figure 3a, creating sections with asymmetric type of contacts. This is confirmed by the AFM topography profile along the suspended nanowire (Figure 3c). The SThM image (inset to Figure 3c, with the temperature profile shown in Figure 3d) of this suspended device shows completely different temperature variations than those of substrate-supported devices. Particularly, the temperature is lowest in the region when the nanowire makes contact with the substrate, and the highest temperature is in the middle of the suspended section. This

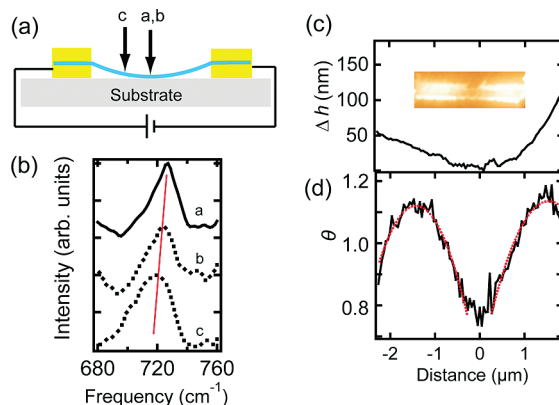


Figure 3. (a) Schematics of the suspended nanowire device; (b) spatially resolved Raman spectra of the A_1 LO phonon mode with the spectrum a taken under the zero-bias (power) condition and spectra b and d taken along the biased nanowire with positions indicated in (a), and the spectra are shifted vertically for clarity; (c) the topography profile (Δh) along the suspended nanowire with the height of the nanowire subtracted, and the inset shows the corresponding SThM image; (d) the temperature profile (black solid line) of the SThM image shown in the inset to (c) with the red dotted lines representing the fitting results using eq 4.

is also confirmed by spatially resolved Raman studies with the spectra shown in Figure 3b. The relative significance between nanowire–substrate and nanowire–electrode heat dissipation can be seen from the temperature difference at these two interfaces. Consistent with the analysis on substrate-supported nanowires, the lower temperature at the nanowire–substrate contact region, compared to that at the nanowire–electrode interface, clearly demonstrates the dominant role of the former in dissipating heat.⁵⁶ This sample geometry also allows an estimation of the nanowire thermal conductivity. In particular, with $G = 0$ for the suspended section, the solution to eq 1, with the left electrode at $x = 0$, is given by

$$\theta(x) = \frac{T(x) - T_0}{T_{\text{avg}} - T_0} = -\frac{Q}{2kA(T_{\text{avg}} - T_0)L}x^2 + \left[\frac{Q}{2kA(T_{\text{avg}} - T_0)} + \frac{T_{e,2} - T_{e,1}}{(T_{\text{avg}} - T_0)L} \right]x + \frac{T_{e,1} - T_0}{T_{\text{avg}} - T_0} \quad (4)$$

METHODS

Nanowire Growth. A thermal chemical vapor deposition (CVD) system (EasyTube 2000, First Nano) was used for the GaN nanowire growth. Gallium pellets (Alfa Aesar, 99.9999%) and anhydrous NH_3 (99.99%) were used as the gallium and the nitrogen sources, respectively, with the growth temperature of 920 °C and the pressure of 500 Torr. A mixture of Ar and H_2 was used as the carrier gas. These nanowires were grown on c-plane sapphire substrates coated with nickel nitrate hexahydrate (Alfa Aesar, 99.9985%) diluted in ethanol. Single GaN nanowire two-terminal devices were fabricated on silicon substrates coated with a silicon nitride (Si_3N_4) layer (~400 nm thick). Ti/Au electrodes (~1 μm wide) were defined by e-beam lithography followed by metallization (via sputtering) and lift-off. For suspended nanowire device fabrications, nanowires were first dis-

persed on PMMA-coated substrate followed by the e-beam lithography. The metallization was carried out with samples mounted at the 45° angle to the metal target under continuous rotation during the sputtering process.

SThM Measurements. Scanning thermal microscopy was performed on an atomic force microscope (CryoView 2000, Nanonics) using thermoresistive probes mounted on quartz tuning forks (schematics shown in Figure 1a) with a normal-force feedback mechanism. The intermittent contact mode was used, which was necessary to minimize the mechanical interaction between nanowires and the probe; this was especially important for studying suspended nanowire devices. The thermal probe consists of two Pt wires running through a glass fiber. The fused Pt wire junction, which protrudes out of the fiber, acts as the heat sensor. With a small amount of current (~0.1 mA) through the Pt wire junction, the change in the electrical resistance of this

junction, obtained by measuring the voltage change across a Wheatstone bridge (ΔV_{th}), corresponds to the temperature variations at the wire junction.

Raman Measurements. For spatially resolved single nanowire Raman spectroscopy, the optical excitation was provided by the 442 nm emission from a He–Cd laser (Kimmion), and an optical microscope coupled to a Raman spectrometer (InVia, Renishaw) was used to focus the laser beam to a diffraction-limited spot. An optical microscope hot stage (HCS302, Instec) was used to carry out variable-temperature Raman spectroscopy measurements.

Supporting Information Available: Model of A₁ LO phonon frequency (ω_{LO}) as a function of temperature. This material is available free of charge via the Internet at <http://pubs.acs.org>.

REFERENCES AND NOTES

- Pop, E.; Sinha, S.; Goodson, K. E. Heat Generation and Transport in Nanometer-Scale Transistors. *Proc. IEEE* **2006**, *94*, 1587–1601.
- Mahajan, R.; Chiu, C. P.; Chrysler, G. Cooling a Microprocessor Chip. *Proc. IEEE* **2006**, *94*, 1476–1486.
- P Pop, E.; Sinha, S.; Goodson, K. E. Thermal Phenomena in Nanoscale Transistors (reprinted from the IEEE Itherm 2004 Proceedings—the Ninth Intersociety Conference on Thermal and Thermomechanical Phenomena in Electronic Systems, June 1–4, 2004, Las Vegas, NV USA). *J. Electron. Packaging* **2006**, *128*, 102–108.
- Qian, F.; Li, Y.; Gradecak, S.; Wang, D. L.; Barrelet, C. J.; Lieber, C. M. Gallium Nitride-Based Nanowire Radial Heterostructures for Nanophotonics. *Nano Lett.* **2004**, *4*, 1975–1979.
- Kuykendall, T.; Ulrich, P.; Aloni, S.; Yang, P. Complete Composition Tunability of InGaN Nanowires Using a Combinatorial Approach. *Nat. Mater.* **2007**, *6*, 951–956.
- Qian, F.; Li, Y.; Gradecak, S.; Park, H. G.; Y.; Dong, J.; Ding, Y.; Wang, Z. L.; Lieber, C. M. Multi-Quantum-Well Nanowire Heterostructures for Wavelength-Controlled Lasers. *Nat. Mater.* **2008**, *7*, 701–706.
- Gradecak, S.; Qian, F.; Li, Y.; Park, H. G.; Lieber, C. M. GaN Nanowire Lasers with Low Lasing Thresholds. *Appl. Phys. Lett.* **2005**, *87*, 173111–3.
- Daumiller, I.; Kirchner, C.; Kamp, M.; Ebeling, K. J.; Kohn, E. Evaluation of the Temperature Stability of AlGaN/GaN Heterostructure FETs. *IEEE Electron Device Lett.* **1999**, *21*, 448–450.
- Guthy, C.; Nam, C. Y.; Fischer, J. E. Unusually Low Thermal Conductivity of Gallium Nitride Nanowires. *J. Appl. Phys.* **2008**, *102*, 064319–8.
- Zou, J. Lattice Thermal Conductivity of Freestanding Gallium Nitride Nanowires. *J. Appl. Phys.* **2010**, *108*, 034324–7.
- Westover, T.; Jones, R.; Huang, J. Y.; Wang, G.; Lai, E.; Talin, A. A. Photoluminescence, Thermal Transport, and Breakdown in Joule-Heated GaN Nanowires. *Nano Lett.* **2009**, *9*, 257–263.
- Prasher, R. Predicting the Thermal Resistance of Nanosized Constrictions. *Nano Lett.* **2005**, *5*, 2155–2159.
- Cahill, D. G.; Goodson, K.; Majumdar, A. Thermometry and Thermal Transport in Micro/Nanoscale Solid-State Devices and Structures. *J. Heat Transfer* **2002**, *124*, 223–241.
- Cahill, D. G.; Ford, W. K.; Goodson, K. E.; Mahan, G. D.; Majumdar, A.; Maris, H. J.; Merlin, R.; Phillpot, S. R. Nanoscale Thermal Transport. *J. Appl. Phys.* **2003**, *93*, 793–818.
- Majumdar, A. *Annu. Rev. Mater. Sci.* **1999**, *29*, 505–585.
- Hsu, I. K.; Kumar, R.; Bushmaker, A.; Cronin, S. B.; Pettes, M. T.; Shi, L.; Brintlinger, T.; Fuhrer, M. S.; Cumings, J. Optical Measurement of Thermal Transport in Suspended Carbon Nanotubes. *Appl. Phys. Lett.* **2008**, *92*, 063119–3.
- Freitag, M.; Steiner, M.; Martin, Y.; Perebeinos, V.; Chen, Z. H.; Tsang, J. C.; Avouris, P. Energy Dissipation in Graphene Field-Effect Transistors. *Nano Lett.* **2009**, *9*, 1883–1888.
- Doerk, G. S.; Carraro, C.; Maboudian, R. Single Nanowire Thermal Conductivity Measurements by Raman Thermography. *ACS Nano* **2010**, *4*, 4908–4914.
- Bae, M.-H.; Ong, Z.-Y.; Estrada, D.; Pop, E. Imaging, Simulation, and Electrostatic Control of Power Dissipation in Graphene Devices. *Nano Lett.* **2010**, *10*, 4787–4793.
- Freitag, M.; Chiu, H. Y.; Steiner, M.; Perebeinos, V.; Avouris, P. Thermal Infrared Emission from Biased Graphene. *Nat. Nanotechnol.* **2010**, *5*, 497–501.
- Paddock, C. A.; Eesley, G. L. Transient Thermoreflectance from Thin Metal-Films. *J. Appl. Phys.* **1986**, *60*, 285–290.
- Epperlein, P. W. Micro-Temperature Measurements on Semiconductor-Laser Mirrors by Reflectance Modulation—A Newly Developed Technique for Laser Characterization. *Jpn. J. Appl. Phys.* **1993**, *32*, 5514–5522.
- Shi, L.; Plyasunov, S.; Bachtold, A.; McEuen, P. L.; Majumdar, A. Scanning Thermal Microscopy of Carbon Nanotubes Using Batch-Fabricated Probes. *Appl. Phys. Lett.* **2000**, *77*, 4295–4297.
- Sadat, S.; Tan, A.; Chua, Y. J.; Reddy, P. Nanoscale Thermometry Using Point Contact Thermocouples. *Nano Lett.* **2010**, *10*, 2613–2617.
- Shi, L.; Zhou, J. H.; Kim, P.; Bachtold, A.; Majumdar, A.; McEuen, P. L. Thermal Probing of Energy Dissipation in Current-Carrying Carbon Nanotubes. *J. Appl. Phys.* **2009**, *105*, 104306–5.
- Shi, L.; Majumdar, A. Thermal Transport Mechanisms at Nanoscale Point Contacts. *J. Heat Transfer* **2002**, *124*, 329–337.
- Soudi, A.; Khan, E. H.; Dickinson, J. T.; Gu, Y. Observation of Unintentionally Incorporated Nitrogen-Related Complexes in ZnO and GaN Nanowires. *Nano Lett.* **2009**, *9*, 1844–1849.
- Shealy, J. R.; Prunty, T. R.; Chumbes, E. M.; Ridley, B. K. Growth and Passivation of AlGaN/GaN Hetero Structures. *J. Cryst. Growth* **2003**, *250*, 7–13.
- Boulay, S.; Touati, S.; Sar, A. A.; Hoel, V.; Gaquiere, C.; De Jaeger, J. C.; Joblot, S.; Cordier, Y.; Semond, F.; Massies, J. AlGaN/GaN HEMTS on a (001)-Oriented Silicon Substrate Based on 100-nm SiN Recessed Gate Technology for Microwave Power Amplification. *IEEE Trans. Electron Devices* **2007**, *54*, 2843–2848.
- Kim, G. T.; Gu, G.; Waizmann, U.; Roth, S. Simple Method To Prepare Individual Suspended Nanofibers. *Appl. Phys. Lett.* **2002**, *80*, 1815–1817.
- Dames, C.; Chen, G. Theoretical Phonon Thermal Conductivity of Si/Ge Superlattice Nanowires. *J. Appl. Phys.* **2004**, *95*, 682–693.
- Moore, A. L.; Saha, S. K.; Prasher, R. S.; Shi, L. Phonon Backscattering and Thermal Conductivity Suppression in Sawtooth Nanowires. *Appl. Phys. Lett.* **2008**, *93*, 083112–3.
- Kim, P.; Shi, L.; Majumdar, A.; McEuen, P. L. Mesoscopic Thermal Transport and Energy Dissipation in Carbon Nanotubes. *Physica B* **2002**, *323*, 67–70.
- Luo, K.; Shi, Z.; Varesi, J.; Majumdar, A. Sensor Nanofabrication, Performance, and Conduction Mechanisms in Scanning Thermal Microscopy. *J. Vac. Sci. Technol. B* **1997**, *15*, 349–360.
- We note that, since our SThM works in the intermittent contact mode, forced air convection might also be a factor.
- Xu, J. B.; Lauger, K.; Moller, R.; Dransfeld, K.; Wilson, I. H. Heat-Transfer between Two Metallic Surfaces at Small Distances. *J. Appl. Phys.* **1994**, *76*, 7209–7216.
- At the vacuum of 10^{-6} Torr, a residual liquid layer might still be present on the sample surface. However, the intermittent contact mode used here should lead to a decreased contribution from the heat conduction through the liquid bridge. Moreover, the relatively high temperature (~ 100 °C, see also the text) in the nanowire in this case decreases the coverage of liquid film on the nanowire, and thus further diminishes the liquid heat conduction.
- This is different from what has been suggested in previous studies,^{23,26,34} where the contribution of the liquid

conduction was found to be at least comparable to that of the solid–solid conduction.

39. Mulet, J. P.; Joulain, K.; Carminati, R.; Greffet, J. J. Nanoscale Radiative Heat Transfer between a Small Particle and a Plane Surface. *Appl. Phys. Lett.* **2001**, *78*, 2931–2933.
40. Rousseau, E.; Siria, A.; Jourdan, G.; Volz, S.; Comin, F.; Chevrier, J.; Greffet, J. J. Radiative Heat Transfer at the Nanoscale. *Nat. Photonics* **2009**, *3*, 514–517.
41. Hinz, M.; Marti, O.; Gotsmann, B.; Lantz, M. A.; Durig, U. High Resolution Vacuum Scanning Thermal Microscopy of HfO_2 and SiO_2 . *Appl. Phys. Lett.* **2008**, *92*, 043122–3.
42. This model assumes a constant k as a function of temperature. We note that, while the temperature dependence of k in bulk GaN is well known, we are not aware of any reports, experimental or theoretical, for the case of GaN nanowires at high temperatures (higher than the room temperature), the characteristics of which can be significantly different than those in bulk. In ref 9, the extrapolation of both experimental and theoretical results on GaN nanowires (with diameters >90 nm) obtained at low temperatures suggests a relative constant k at high temperatures, at least below 400 K, which is approximately the highest temperature in our nanowire devices (see also the text). In addition, this model also ignores heat dissipation in nanowires through air conduction, convection, and radiation. The significance of these heat dissipation mechanisms have been shown to be minimal in nanoscale devices (see ref 11 and Hsu, I. K.; Pows, M. T.; Bushmaker, A.; Aykol, M.; Shi, L.; Cronin, S. B. *Nano Lett.* **2009**, *9*, 590–594).
43. Li, W. S.; Shen, Z. X.; Feng, Z. C.; Chua, S. J. Temperature Dependence of Raman Scattering in Hexagonal Gallium Nitride Films. *J. Appl. Phys.* **2000**, *87*, 3332–3337.
44. Chen, X. B.; Huso, J.; Morrison, J. L.; Bergman, L.; Purdy, A. P. Temperature Response and Anharmonicity of the Optical Phonons in GaN Nanowires. *J. Appl. Phys.* **2005**, *98*, 026106–3.
45. Since the laser excitation energy is below the bandgap of GaN, minimal laser heating is expected in these nanowires.
46. While we were only able to measure the temperature using Raman close to the center of the nanowire channel due to the laser heating of the electrodes, if we assume that the SThM signal (ΔV_{th}) is proportional to the temperature (ref 23), then we can also estimate the temperatures at electrodes for calculating the average temperature over the entire nanowire channel. We note that, since the temperature is constant over the most of nanowire channel for substrate-supported devices, the contribution from temperature variations in small regions (close to the electrodes) toward T_{avg} is expected to be small.
47. G has contributions from the nanowire/ Si_3N_4 interface thermal resistance and the spreading resistance in Si_3N_4 thin film and the Si substrate. As the values of G determined here are similar to those obtained (see also the text) for interfaces between GaN and various substrates (Si, SiC, and sapphire), which have significantly different thermal conductivities, this indicates that the interface thermal resistance, instead of the spreading resistance in the substrate material, is the main contribution to G .
48. Florescu, D.; Asnin, V. M.; Pollak, F. H.; Molnar, R. J.; Wood, C. E. C. High Spatial Resolution Thermal Conductivity and Raman Spectroscopy Investigation of Hydride Vapor Phase Epitaxy Grown n-GaN/Sapphire (0001): Doping Dependence. *J. Appl. Phys.* **2000**, *88*, 3295–3300.
49. Tham, D.; Nam, C. Y.; Fischer, J. E. Defects in GaN Nanowires. *Adv. Funct. Mater.* **2006**, *16*, 1197–1202.
50. Liu, J.; Meng, X. M.; Jiang, Y.; Lee, C. S.; Bello, I.; Lee, S. T. Gallium Nitride Nanowires Doped with Silicon. *Appl. Phys. Lett.* **2003**, *83*, 4241–4243.
51. Kuzmik, J.; Bychikhin, S.; Pogany, D.; Gaquiere, C.; Pichonat, E.; Morvan, E. Investigation of the Thermal Boundary Resistance at the III-Nitride/Substrate Interface Using Optical Methods. *J. Appl. Phys.* **2007**, *101*, 054508–6.
52. Sarua, A.; Ji, H.; Hilton, K. P.; Wallis, D. J.; Uren, M. J.; Martin, T.; Kuball, M. Thermal Boundary Resistance between GaN and Substrate in AlGaN/GaN Electronic Devices. *IEEE Trans. Electron Devices* **2007**, *54*, 3152–3158.
53. Turin, V. O.; Balandin, A. A. Performance Degradation of GaN Field-Effect Transistors Due to Thermal Boundary Resistance at GaN/Substrate Interface. *Electron. Lett.* **2004**, *40*, 81–83.
54. Eckhouse, T. A.; Suzer, O.; Kurdak, C.; Yun, F.; Morkoc, H. Electric-Field-Induced Heating and Energy Relaxation in GaN. *Appl. Phys. Lett.* **2003**, *82*, 3035–3037.
55. Kedzierski, J.; leong, M.; Nowak, E.; Kanarsky, T. S.; Zhang, Y.; Roy, R.; Boyd, D.; Fried, D.; Wong, H. S. P. Extension and Source/Drain Design for High-Performance FinFET Devices. *IEEE Trans. Electron Devices* **2003**, *50*, 952–958.
56. The thermal resistances at the nanowire–electrode and nanowire–substrate interfaces also depend on the interface area. Here, for suspended nanowires, from a rough estimate, the length of the nanowire–substrate interface is ≤ 1 μm , thus the area of this interface is comparable or smaller than that of the wire–electrode interface (length ~ 1 μm).
57. Here, we assume that the mechanical bending of the nanowire does not significantly change k . For the device shown in Figure 3c,d, the right electrode is higher than the left one, resulting in different degrees of bending in the two suspended sections. However, the temperature spatial variations in these two sections are relatively similar, supporting, at least to some degree, this assumption. We note that, in standard nanowire thermal conductivity measurements using the suspended configuration, such a mechanical bending is also expected to be present.